Journal of Materials Chemistry A

ROYAL SOCIETY OF CHEMISTRY

PAPER

View Article Online
View Journal | View Issue

Check for updates

Cite this: *J. Mater. Chem. A*, 2025, **13**, 13789

Supramolecular organic framework nanosheets for efficient singlet oxygen generation: a multilevel energy transfer approach for photocatalytic Minisci reactions†

Jian-Yue Liu,[a] Rong-Zhen Zhang,[a] Ning Han,[*b] Hui Liu*[a] and Ling-Bao Xing[*a]

Received 22nd February 2025
Accepted 30th March 2025

DOI: 10.1039/d5ta01483b

rsc.li/materials-a

Replicating the multistep and sequential energy transfer observed in natural photosynthesis, the development of artificial light-harvesting systems (LHSs) capable of sequential multistep energy transfer remains a challenging and active area of research. In the present work, we have designed and synthesized a triphenylamine-modified cyanophenylenevinylene derivative (TPCI), which can self-assemble with cucurbit[8]uril (CB[8]) *via* host–guest interactions to form a supramolecular organic framework (SOF). The structural restrictions of its macrocyclic framework greatly enhance the fluorescence emission intensity of the SOF compared to the monomeric TPCI molecule, rendering it an optimal energy donor and pertinent for the advancement of light-harvesting systems (LHSs). Utilizing the SOF as the energy donor, we identified two distinct cyanine dyes (Cy5 and IR) and successfully developed a sequential light-harvesting system (LHS) from SOF to Cy5, followed by IR with high energy transfer efficiency. Through stepwise energy transfer, the singlet oxygen ($^1O_2$) generation efficiency is progressively enhanced, which exhibited remarkable catalytic efficiency in the Minisci-type alkylation reaction. This study provides a thorough investigation into the development of sequential energy transfer in SOFs as type II photosensitizers for photocatalytic organic transformations.

Introduction

Given the escalating global demand for sustainable energy, solar energy is acknowledged as a vital solution to the energy problem and the mitigation of carbon emissions, due to its enduring sustainability and environmental advantages. Natural photosynthesis, an essential mechanism in transforming solar energy into chemical energy, is vital to the global material cycle.[1] It functions as an effective model for the efficient harnessing of solar energy, incorporating essential processes such as light absorption, energy transfer, and conversion into useful forms.[2] The light-harvesting process, as the preliminary phase of photosynthesis, is crucial for the efficient utilization of solar energy.[3] Inspired by this natural phenomenon, a growing number of researchers are committed to creating light-harvesting systems (LHSs) that seek to emulate the principles of natural photosynthesis.[4,5] Förster resonance energy transfer (FRET) is a commonly employed energy transfer method in the development of artificial systems, in which energy is conveyed from an excited-state donor to a dye acceptor.[6–8] FRET can be utilized to create artificial light-harvesting systems (ALHSs) by incorporating a limited quantity of acceptor molecules into the energy donor system.

In recent years, numerous supramolecular assemblies have been developed utilizing supramolecular self-assembly techniques for application in ALHSs, including metal coordination complexes,[9–20] supramolecular polymers,[21–29] host–guest molecular assemblies,[30–48] micelles,[49–54] vesicles,[55–57] and other structures.[58–60] The supramolecular self-assembly approach is distinguished by its simplicity in building, great efficiency in assembly, and the capacity for precise control over both structure and function. Owing to noncovalent interactions and spatial structural effects, the construction of supramolecular assemblies with precise spatial arrangements enhances the dispersion of fluorescent molecules and mitigates energy losses from chromophore aggregation quenching. Furthermore, the dynamic and controllable characteristics of supramolecular systems, along with the tunability of internal structural space and molecular distances, ensure that the distances between donors and acceptors are maintained within an optimal range, thereby facilitating efficient FRET process.[61–66] Consequently, supramolecular organic frameworks (SOFs), characterized by their periodic pore architectures, uniform solubility, pore-channel development during packing, straightforward synthesis, and simple functional

[a]*School of Chemistry and Chemical Engineering, Shandong University of Technology, Zibo 255000, P. R. China. E-mail: liuhui@sdut.edu.cn; lbxing@sdut.edu.cn*

[b]*Department of Electrical and Computer Engineering, University of Toronto, Toronto, ON M5S 1A4, Canada. E-mail: n.han@utoronto.ca*

† Electronic supplementary information (ESI) available. See DOI: https://doi.org/10.1039/d5ta01483b

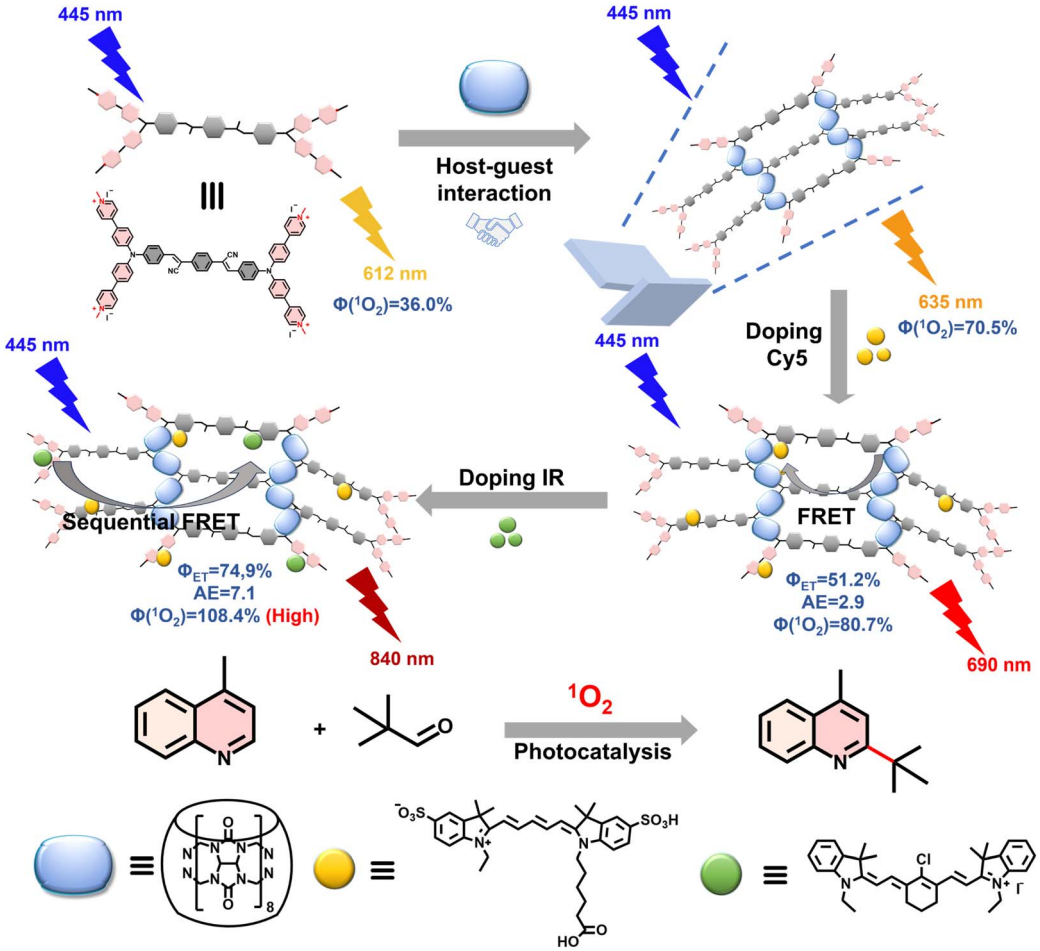

Scheme 1 Schematic diagram of sequential energy transfer process in SOFs for photocatalytic Minisci-type alkylation reaction.

modification, present a promising approach for the construction of high-efficiency ALHSs.[46,47]

This study involved the design and synthesis of a triphenylamine-modified cyanophenylenevinylene derivative (TPCI), which establishes a supramolecular organic framework (SOF) *via* host–guest interactions with cucurbit[8]uril (CB[8]) in the aqueous solution. The structural constraints of its macrocyclic framework significantly amplify the fluorescence emission intensity of the SOF in comparison to the monomeric TPCI molecule, establishing it as an ideal energy donor and relevant for the development of light-harvesting system (LHS). Utilizing the SOF as the energy donor, we identified two distinct cyanine dyes (Cy5 and IR) and successfully developed a sequential LHS from SOF to Cy5, followed by IR. The synthesized LHS demonstrated a significant enhancement in singlet oxygen ($^1O_2$) production and exhibited remarkable catalytic efficiency in the Minisci-type alkylation reaction (Scheme 1).

Experimental

Synthesis of compound TPCI

In a 50 mL round-bottom flask, compound TPC (200.0 mg, 0.20 mmol) and methyl iodide (4.8 g, 2.0 mL, 34.0 mmol) were dissolved in 30 mL acetonitrile. The mixture was stirred and heated to 40 °C for 1 h and then refluxed for 12 h. After cooling to room temperature, the mixture was poured into diethyl ether to get precipitates. The precipitates were then washed with diethyl ether three times and dried under reduced pressure to afford the product as an orange powder (244 mg, yield: 79%). ^{1}H NMR (400 MHz, DMSO-d_6) δ 8.98 (s, 8H), 8.49 (s, 8H), 8.18 (s, 2H), 8.15 (d, J = 8.1 Hz, 8H), 8.07 (s, 4H), 7.93 (s, 4H), 7.37 (s, 12H), 4.32 (s, 12H). ^{13}C NMR (101 MHz, DMSO-d_6) δ 153.14, 149.21, 145.54, 131.38, 129.99, 128.57, 126.48, 123.28, 47.03. HRMS: m/z calculated for $C_{72}H_{58}N_8^{4+}$, 258.8275; found: 258.6193.

Results and discussion

The target compound TPCI was synthesised through a four-step reaction, with both intermediates and products confirmed *via* ^{1}H NMR, ^{13}C NMR, and HRMS (Scheme S1 and Fig. S1–S6†). Initially, the fluorescence properties of TPCI were investigated using fluorescence emission spectra in solvents with varying dimethyl sulfoxide (DMSO) and H_2O ratios. As illustrated in Fig. S7,† TPCI showed weak fluorescence emission in DMSO; however, as the water content increased from 0 to 100%, its

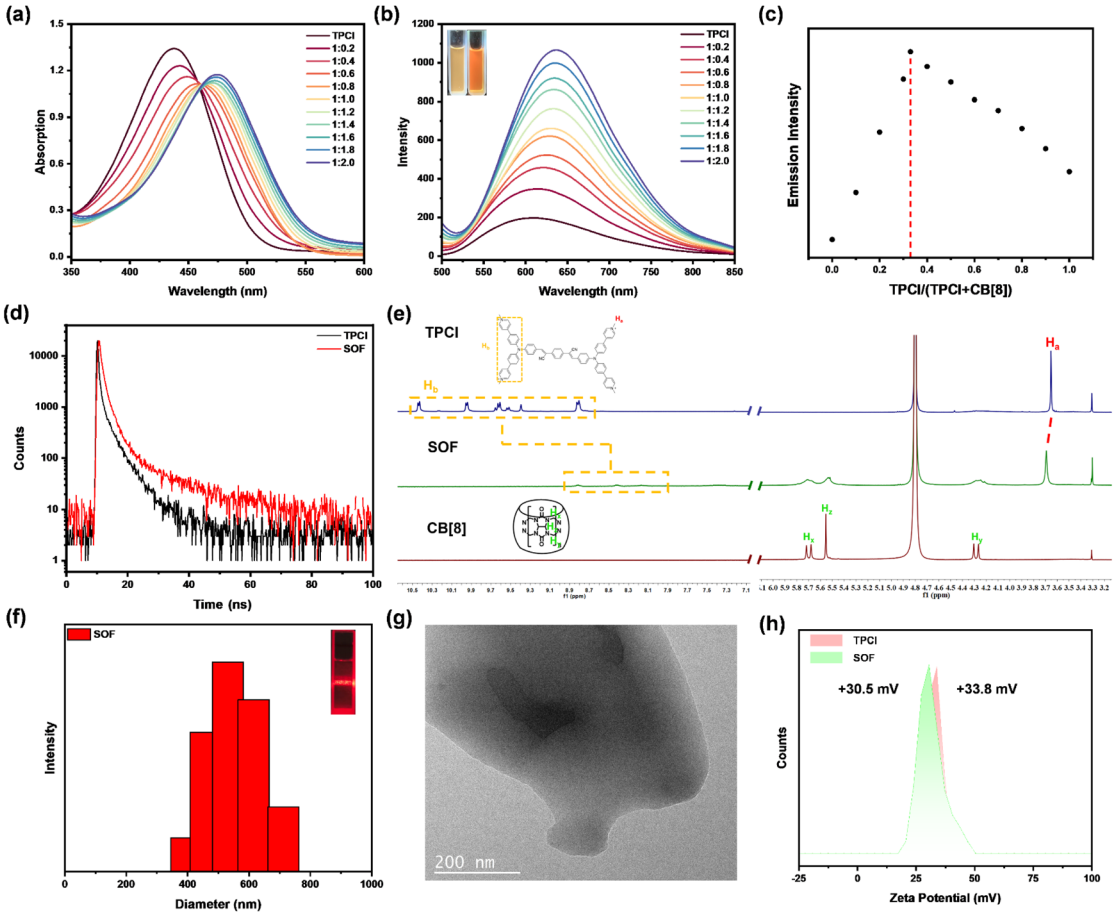

Fig. 1 (a) UV-Vis absorption spectra and (b) fluorescence emission spectra of TPCl before and after adding CB[8] (inset: color changes of TPCl and SOF); (c) Job's plot of TPCl and CB[8]; (d) fluorescence lifetime of TPCl and SOF; (e) ^{1}HNMR titration spectra of TPCl with CB[8] in D_2O; (f) particle size of SOF (inset: Tyndall effect of SOF); (g) TEM image of SOF; (h) zeta potential of TPCl before and after the addition of 2.0 equiv. CB[8].

fluorescence emission markedly intensified. Concurrently, TPCl exhibited orange-yellow fluorescence in the aqueous phase, indicating its aggregation-induced emission (AIE) effect (Fig. S7†). The assembly behaviour of TPCl and CB[8] in aqueous solution was further examined using UV-Vis absorption spectra, fluorescence emission spectra, and ^{1}H NMR titration experiments. As illustrated in Fig. 1a, the incorporation of CB[8] resulted in a progressive attenuation of TPCl absorption at 445 nm, accompanied by a redshift. Simultaneously, the fluorescence emission spectra revealed a considerable rise in the fluorescence intensity of TPCl at 612 nm, which redshifted to 635 nm, a behaviour likely resulting from the host–guest interaction between TPCl and CB[8] (Fig. 1b). Upon the addition of 2.0 equiv. of CB[8], TPCl exhibited its maximum fluorescence emission intensity, with a colour transition from orange-yellow to orange (Fig. S7†). Subsequently, Job's plots were used to ascertain the stoichiometric ratio between TPCl and CB[8] in SOF (Fig. 1c). As the concentration ratio of TPCl was incrementally increased, the maximum fluorescence intensity was recorded at 0.33, indicating a stoichiometric ratio of TPCl to CB[8] of 1 : 2, while the total concentrations of TPCl and CB[8] remained constant. In comparison to the state before to the introduction of CB[8], the fluorescence lifespan of SOF rose from 1.68 ns to 1.93 ns (Fig. 1d), while the fluorescence quantum yield (Φ_f) increased from 1.5% to 1.9% (Table S1†). Furthermore, ^{1}H NMR titration experiments were conducted to investigate the host–guest interaction between TPCl and CB[8]. Upon the addition of 2.0 equiv. of CB[8] to the D_2O solution of TPCl (Fig. 1e), the characteristic signal of the methyl group of TPCl (H_a) exhibited a downfield shift, while the signal in the aromatic region (H_b) displayed an upfield shift. Additionally, the characteristic signal of CB[8] became broadened, signifying the successful encapsulation of the methylated pyridine unit of TPCl within the cavity of CB[8] *via* host–guest interaction, thus forming a stable SOF.

Thereafter, the morphology of SOF was analysed utilizing dynamic light scattering (DLS) and transmission electron microscopy (TEM). The DLS test results revealed that the introduction of CB[8] into the TPCl solution resulted in an average size of approximately 500 nm (Fig. 1f). Upon laser illumination, a pronounced Tyndall effect was observed, signifying the formation of substantial aggregate SOF in the aqueous solution. Subsequently, TEM analysis was employed to examine the structure of SOF. Fig. 1g illustrates the observation of a two-dimensional nanosheet structure of SOF, with a diameter that aligns with the measurements obtained using DLS, thereby

validating the creation of SOF. Furthermore, the Zeta potential of TPCI altered from +33.8 to +30.5 mV following the incorporation of CB[8], hence reinforcing the successful formation of SOF (Fig. 1h). The aforementioned data unequivocally indicate that TPCI and CB[8] generate SOF in the aqueous solution.

Owing to the exceptional fluorescence properties of SOF in the aqueous solution, it can function as the energy donor for the development of LHS. The energy level compatibility between the fluorescence acceptor and the donor is crucial in the FRET process. Consequently, in the initial phase of energy transfer, Cy5 was selected as the energy acceptor due to a significant overlap between the absorption spectrum of Cy5 (550–690 nm) and the emission spectrum of SOF (520–800 nm) (Fig. S8a†). The incremental addition of Cy5 resulted in a fluorescence emission peak at 690 nm, indicative of Cy5's fluorescence emission (Fig. 2a). Simultaneously, the emission peak of SOF at 635 nm diminished markedly, indicating that the energy of SOF was sent to Cy5 *via* the FRET mechanism. Furthermore, the CIE 1931 color coordinates clearly demonstrated that the fluorescence color transitioned from orange to orange-red with the incorporation of Cy5 (Fig. S9†). Additionally, we investigated the energy transfer mechanism of LHS by fluorescence lifespan analyses. Following the initial phase of energy transfer, the fluorescence lifespan diminished from 1.93 ns to 1.80 ns (Fig. 2c), while the fluorescence quantum yield increased from 1.9% to 10.1% (Table S1†). The results indicate that energy was transferred from SOF to the acceptor Cy5. At a donor (SOF) to acceptor (Cy5) ratio of 1 : 0.012, the energy transfer efficiency (Φ_{ET}) was 51.2%, and the antenna effect (AE) was 2.9 (Fig. S10a and b†).

Natural photosynthesis is generally a multi-stage process. Therefore, to enhance the simulation of natural photosynthesis, we used IR dye as the secondary sequential energy acceptor. IR has an absorption band between 600 and 800 nm in water, which substantially coincides with the emission band of SOF + Cy5 (Fig. S8b†). After the addition of IR to the aqueous solution of SOF + Cy5, the emission intensity at 840 nm of the SOF + Cy5 aqueous solution gradually increased, coinciding with the emission peak of IR (Fig. 2b), and the fluorescence intensity at 690 nm of SOF + Cy5 decreased, indicating the occurrence of two-step sequential energy transfer. Concurrently, the CIE 1931 chromaticity coordinates indicated that during the two-step sequential energy transfer, the fluorescence color shifted from orange-red to red (Fig. S9†). Moreover, with the application of IR, the fluorescence lifetime diminished from 1.80 ns to 1.39 ns (Fig. 2c), while the fluorescence quantum yield increased from 10.1% to 13.5% (Table S1†). Upon mixing SOF + Cy5 (donor) and IR (acceptor) at a molar ratio of 1 : 0.012 : 0.16, the computed Φ_{ET} and AE were 74.9% and 7.1, respectively (Fig. S10c and d†). These data indicate that the integration of IR established an LHS *via* a two-step sequential energy transfer process.

We examined the potential applications of LHS in improving the photocatalytic oxidation process. 9,10-Anthracenediyl-bis(methylene)dimalonic acid (ABDA) was utilized as a selective detection reagent for $^1O_2$ (Fig. S11†). Upon the addition of ABDA to the aqueous solutions of TPCI, SOF, SOF + Cy5, and SOF + Cy5 + IR, the distinctive peaks of ABDA in these solutions diminished under blue light irradiation. The most pronounced reduction was observed in SOF + Cy5 + IR, suggesting that SOF + Cy5 + IR produced a greater quantity of $^1O_2$ (Fig. 2d). We subsequently assessed the quantum yield of $^1O_2$ utilizing Rose Bengal (RB) as a reference (Fig. S12†). The findings revealed that the quantum yields of $^1O_2$ for TPCI, SOF, SOF + Cy5, and SOF +

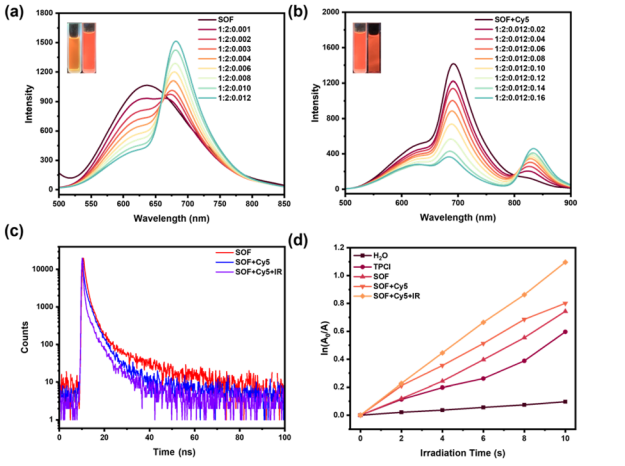

Fig. 2 (a) Fluorescence emission spectra of SOF after adding Cy5 (inset: color changes of SOF and SOF + Cy5); (b) fluorescence emission spectra of SOF + Cy5 after adding IR (inset: color changes of SOF + Cy5 and SOF + Cy5 + IR); (c) fluorescence lifetime curves of SOF, SOF + Cy5, and SOF + Cy5 + IR; (d) $\Delta_{Abs}(A_0/A)$ of ABDA (1.0×10^{-4} M) under light irradiation (440–450 nm, 5 W) for different photosensitizers at different times.

Table 1 Optimization of the reaction conditions

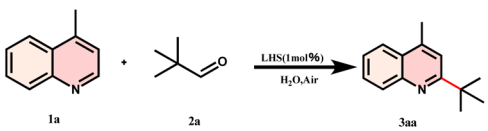

Entry	Variation from standard conditions[a]	Yield[b] (%)
1	None	93
2	TPCI	21
3	SOF	47
4	SOF + Cy5	66
5	LHS (0.5 mol%)	54
6	LHS (1.5 mol%)	96
7	CB[8]	NR
8	Cy5	Trace
9	IR	NR
10	6 h	44
11	18 h	95
12	No SOF + Cy5 + IR	NR
13	No light	NR
14	Under N_2	NR

[a] Reaction conditions: **1a** (0.2 mmol), **2a** (0.5 mmol), light-harvesting system (LHS): SOF + Cy5 + IR (1.0 mol%), blue LEDs (5 W, λ = 440–450 nm), room temperature (r.t.), under air conditions, 12 h. [b] Isolated yield; NR = no reaction.

Cy5 + IR were 36.0%, 70.5%, 80.7%, and 108.4%, respectively (Fig. S13†), thereby confirming that SOF + Cy5 + IR is an effective type II photosensitizer.

To enhance the simulation of energy transfer in photosynthesis, we examined the appropriateness of this energy transfer system in a Minisci-type reaction. We initially selected 4-methylquinoline (**1a**) and pivalaldehyde (**2a**) as the substrates. The screening assays of the reaction conditions demonstrated that this reaction had exceptional catalytic activity. Table 1 demonstrates that under the excitation of a 440–450 nm LED lamp, the alkylation product **3aa** was achieved in 93% yield with merely 1.0 mol% of the catalyst (entry 1). In contrast, when the individual components of the energy transfer system were employed for independent catalysis of the reaction, exceedingly poor yields or no reaction occurred (entries 2–4 and 7–9), indicating that the energy transfer process is critically significant. Concurrently, it is significant that the catalytic activity of one-step energy transfer diminished markedly (entry 4). In addition, we screened the equivalents of the catalyst. A decrease in the equivalent of the catalyst would result in a reduction of the reaction yield (54%, entry 5). On the contrary, an increase in the equivalent of the catalyst had a negligible effect on the reaction yield (96%, entry 6). Thus, 1.0 mol% was determined as the optimal dosage of the catalyst. Furthermore, the studies revealed that a decrease in reaction time led to a substantial fall in reaction yield (44%, entry 10). Conversely, an increase in reaction time did not significantly affect the reaction yield (95%, entry 11). The conclusive control experiments indicated that the

Table 2 Substrate scope for the Minisci-type alkylation reaction[a,b]

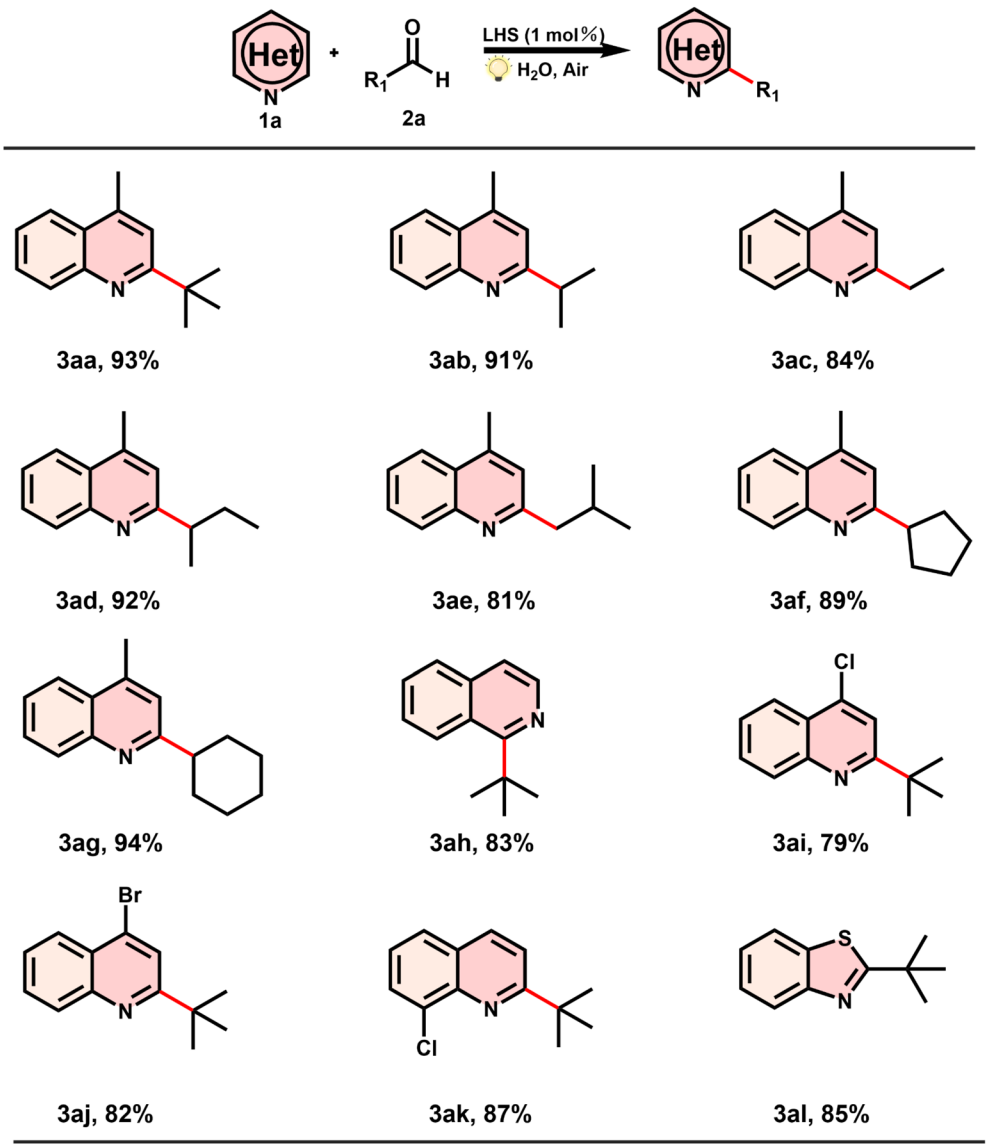

[a] Reaction conditions: **1a** (0.2 mmol), **2a** (0.5 mmol), light-harvesting system (LHS): SOF + Cy5 + IR (1.0 mol%), blue LEDs (5 W, λ = 440–450 nm), room temperature (r.t.), under air conditions, 12 h. [b] Isolated yield.

energy transfer system, illumination, and atmospheric circumstances are pivotal in the process (entries 12–14). The apparent quantum yields (AQY) of products **1a** were calculated to be 0.015%. Upon establishing the optimal reaction conditions, we performed studies to evaluate the compatibility of diverse substrates with the reaction. Table 2 illustrates that a variety of primary aldehydes (**3ac**, **3ae**), secondary aldehydes (**3ab**, **3ad**), tertiary aldehydes (**3aa**), and cycloalkyl aldehydes (**3af**, **3ag**) can be utilized to produce products with moderate to good yields (79–94%) when employing alkyl aldehyde substrates. Unexpectedly, isoquinoline (**3ah**) and benzothiazole (**3al**) also engaged in the reaction effectively (83–85%), thereby confirming the compatibility and catalytic efficacy of this multistep energy transfer system.

We subsequently investigated the photocatalytic mechanism of the decarbonylation Minisci-type alkylation reaction. Initially, we performed experiments to evaluate the inactivation of the substrate for the photosensitizer in an aqueous environment through Stern–Volmer quenching experiment. When only the model substrate **1a** was added, the fluorescence intensity of SOF + Cy5 + IR at 840 nm exhibited nearly no variation. In contrast, when only the model substrate **2a** was introduced, the fluorescence intensity of SOF + Cy5 + IR at 840 nm decreased rapidly. Furthermore, when both the template substrates **1a** and **2a** were simultaneously incorporated into the system, the outcome of the fluorescence intensity assessment was identical to that when only the template substrate **2a** was added. By employing the Stern–Volmer equation $I_0/I = 1 + k_{sv}[Q] = 1 + k_q\tau_0[Q]$, the rate constant was calculated to be 6.52×10^{11} M^{-1} s^{-1}. These results suggest that there exists a strong interaction between the SOF + Cy5 + IR and the template substrate **2a** (Fig. S14†). Control experiments revealed that the introduction of 2,2,6,6-tetramethylpiperidinyloxy (TEMPO) or butylated hydroxytoluene (BHT) into the model reaction significantly inhibited the reaction, implying that it may proceed *via* a radical mechanism (Fig. 3a). Simultaneously, the addition of hole inhibitors, hydroxyl radical inhibitors, and superoxide anion radical ($O_2^{\bullet-}$) inhibitors at conventional reaction conditions resulted in no significant alteration in the reaction yield, suggesting that these chemicals did not participate in the reaction. Furthermore, the introduction of a $^1O_2$ inhibitor (NaN_3) into the reaction system successfully obstructed the reaction, indicating that $^1O_2$ is crucial to the reaction process. Furthermore, the light-switching experiment precluded the chain reaction mechanism (Fig. 3b). Based on the aforementioned mechanistic investigations, we hypothesized a cooperative reaction mechanism for the oxidation of the energy transfer system. Upon light irradiation, the energy transfer mechanism is activated to the excited state (Fig. 3c); thereafter, the excited state SOF* transfers energy to Cy5, which then transfers it to IR. Following a two-step energy transfer, IR attains the excited state IR* and then transfers energy to oxygen, resulting in the formation of $^1O_2$, while IR* returns to the ground state through quenching. Thereafter, pivalaldehyde and $^1O_2$ engage in hydrogen atom transfer (HAT), resulting in the formation of the hydrogen peroxide radical

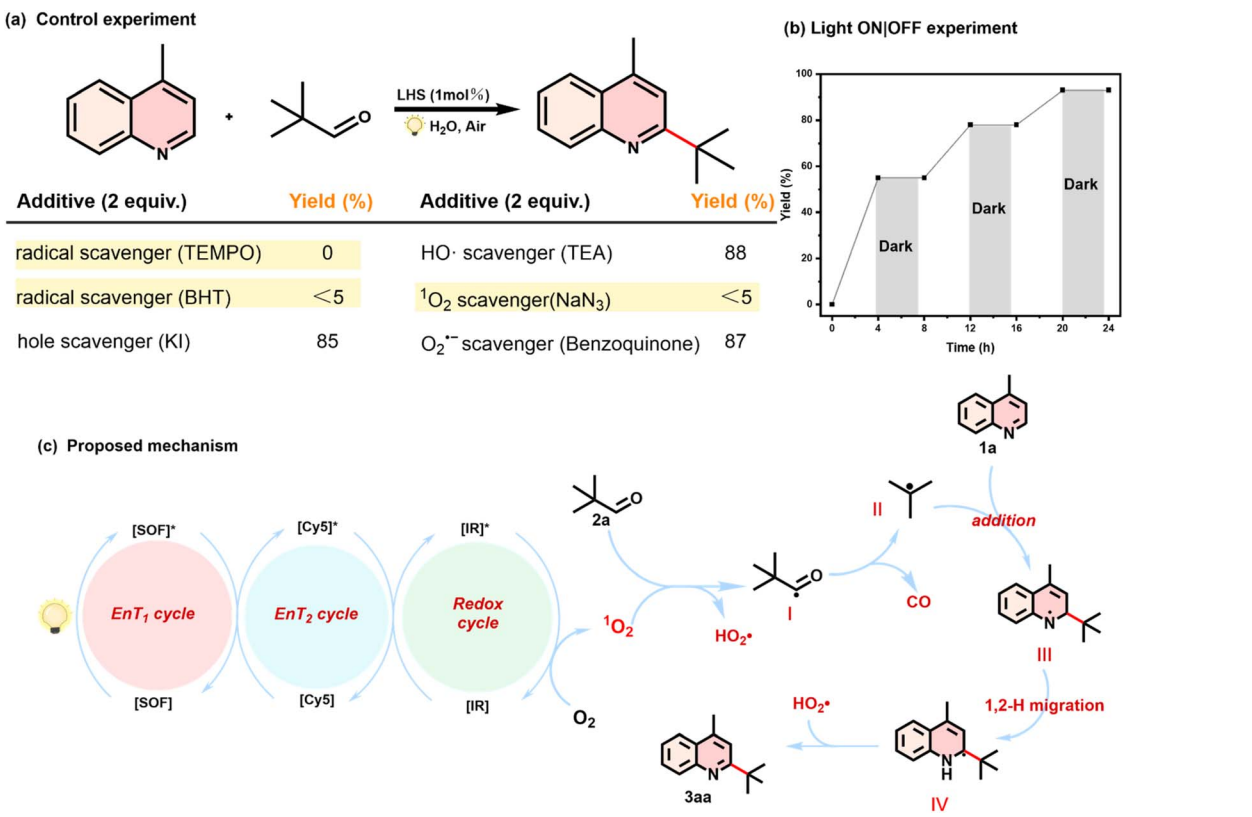

Fig. 3 Mechanistic investigations: (a) control experiment; (b) light on/off experiment; (c) reaction mechanism.

($HO_2^{\bullet}$) and **I**. Subsequently, **I** experience CO loss to produce *tert*-butyl radical, and radical **II** reacts with 4-methylquinoline to yield intermediate radical **III**. Intermediate **III** undergoes a 1,2-hydrogen shift to produce a nitrogen-centered radical intermediate **IV**, which subsequently interacts with $HO_2^{\bullet}$ *via* HAT to yield the desired product.

Conclusions

In conclusion, we have developed a novel LHS that achieves a two-step sequential energy transfer process in the structure of SOF, which can be constructed through host–guest interaction between TPCI and CB[8]. The AIE effect of TPCI, in conjunction with SOF, markedly amplifies the fluorescence emission intensity of TPCI, indicating its potential utility in the development of LHS. Through the utilization of Cy5 and IR as energy acceptors, we have successfully accomplished a consecutive two-step energy transfer process from SOF to Cy5 and then to IR, demonstrating a high energy transfer efficiency and enhanced $^1O_2$ generation capacity, which has greatly facilitated the Minisci-type photooxidation reaction. This study provides a thorough investigation into the development of sequential energy transfer in SOFs as type II photosensitizers for photocatalytic organic transformations.

Data availability

All the data supporting this article have been included in the main text and the ESI.†

Author contributions

Jian-Yue Liu: data curation, formal analysis, investigation, methodology. Rong-Zhen Zhang: data curation, formal analysis. Ning Han: methodology, writing – review & editing. Hui Liu: methodology, resources, writing – review & editing. Ling-Bao Xing: conceptualization, funding acquisition, methodology, project administration, resources, supervision, visualization, writing – review & editing.

Conflicts of interest

There are no conflicts to declare.

Acknowledgements

We are grateful for the financial support from the National Natural Science Foundation of China (52205210), and the Natural Science Foundation of Shandong Province (ZR2022QE033).

Notes and references

1 D. Gust and T. A. Moore, *Science*, 1989, **244**, 35–41.
2 N. E. Holt, D. Zigmantas, L. Valkunas, X.-P. Li, K. K. Niyogi and G. R. Fleming, *Science*, 2005, **307**, 433–436.
3 D.-L. Jiang and T. Aida, *Nature*, 1997, **388**, 454–456.
4 T. Pullerits and V. Sundström, *Acc. Chem. Res.*, 1996, **29**, 381–389.
5 S. Kundu and A. Patra, *Chem. Rev.*, 2017, **117**, 712–757.
6 D. Li, X. Liu, L. Yang, H. Li, G. Guo, X. Li and C. He, *Chem. Sci.*, 2023, **14**, 2237–2244.
7 N. Song, X.-Y. Lou, H. Yu, P. S. Weiss, B. Z. Tang and Y.-W. Yang, *Mater. Chem. Front.*, 2020, **4**, 950–956.
8 H.-Q. Peng, L.-Y. Niu, Y.-Z. Chen, L.-Z. Wu, C.-H. Tung and Q.-Z. Yang, *Chem. Rev.*, 2015, **115**, 7502–7542.
9 H. Lee, Y. H. Jeong, J. H. Kim, I. Kim, E. Lee and W. D. Jang, *J. Am. Chem. Soc.*, 2015, **137**, 12394–12399.
10 C. B. Huang, L. Xu, J. L. Zhu, Y. X. Wang, B. Sun, X. Li and H. B. Yang, *J. Am. Chem. Soc.*, 2017, **139**, 9459–9462.
11 K. Acharyya, S. Bhattacharyya, H. Sepehrpour, S. Chakraborty, S. Lu, B. Shi, X. Li, P. S. Mukherjee and P. J. Stang, *J. Am. Chem. Soc.*, 2019, **141**, 14565–14569.
12 Z. Zhang, Z. Zhao, Y. Hou, H. Wang, X. Li, G. He and M. Zhang, *Angew. Chem., Int. Ed.*, 2019, **58**, 8862–8866.
13 P. Wang, X. Miao, Y. Meng, Q. Wang, J. Wang, H. Duan, Y. Li, C. Li, J. Liu and L. Cao, *ACS Appl. Mater. Interfaces*, 2020, **12**, 22630–22639.
14 Z. Zhang, Z. Zhao, L. Wu, S. Lu, S. Ling, G. Li, L. Xu, L. Ma, Y. Hou, X. Wang, X. Li, G. He, K. Wang, B. Zou and M. Zhang, *J. Am. Chem. Soc.*, 2020, **142**, 2592–2600.
15 P. P. Jia, L. Xu, Y. X. Hu, W. J. Li, X. Q. Wang, Q. H. Ling, X. Shi, G. Q. Yin, X. Li, H. Sun, Y. Jiang and H. B. Yang, *J. Am. Chem. Soc.*, 2021, **143**, 399–408.
16 A. Kumar, R. Saha and P. S. Mukherjee, *Chem. Sci.*, 2021, **12**, 5319–5329.
17 Y. Li, S. S. Rajasree, G. Y. Lee, J. Yu, J.-H. Tang, R. Ni, G. Li, K. N. Houk, P. Deria and P. J. Stang, *J. Am. Chem. Soc.*, 2021, **143**, 2908–2919.
18 K. Acharyya, S. Bhattacharyya, S. Lu, Y. Sun, P. S. Mukherjee and P. J. Stang, *Angew. Chem., Int. Ed.*, 2022, **61**, e202200715.
19 D. Bokotial, K. Acharyya, A. Chowdhury and P. S. Mukherjee, *Angew. Chem., Int. Ed.*, 2024, **63**, e202401136.
20 D. Zhang, W. Yu, S. Li, Y. Xia, X. Li, Y. Li and T. Yi, *J. Am. Chem. Soc.*, 2021, **143**, 1313–1317.
21 M. Kownacki, S. M. Langenegger, S. X. Liu and R. Häner, *Angew. Chem., Int. Ed.*, 2019, **58**, 751–755.
22 C.-L. Sun, H.-Q. Peng, L.-Y. Niu, Y.-Z. Chen, L.-Z. Wu, C.-H. Tung and Q.-Z. Yang, *Chem. Commun.*, 2018, **54**, 1117–1120.
23 J.-J. Li, Y. Chen, J. Yu, N. Cheng and Y. Liu, *Adv. Mater.*, 2017, **29**, 1701905.
24 D. Zhang, Y. Liu, Y. Fan, C. Yu, Y. Zheng, H. Jin, L. Fu, Y. Zhou and D. Yan, *Adv. Funct. Mater.*, 2016, **26**, 7652–7661.
25 C. D. Bosch, S. M. Langenegger and R. Haner, *Angew. Chem., Int. Ed.*, 2016, **55**, 9961–9964.
26 T. Xiao, L. Zhang, H. Wu, H. Qian, D. Ren, Z.-Y. Li and X.-Q. Sun, *Chem. Commun.*, 2021, **57**, 5782–5785.
27 T. Xiao, H. Wu, G. Sun, K. Diao, X. Wei, Z.-Y. Li, X.-Q. Sun and L. Wang, *Chem. Commun.*, 2020, **56**, 12021–12024.
28 H.-Q. Peng, C.-L. Sun, L.-Y. Niu, Y.-Z. Chen, L.-Z. Wu, C.-H. Tung and Q.-Z. Yang, *Adv. Funct. Mater.*, 2016, **26**, 5483–5489.

29 F. Qiao, Z. Yuan, Z. Lian, C.-Y. Yan, S. Zhuo, Z.-Y. Zhou and L.-B. Xing, *Dyes Pigm.*, 2017, **146**, 392–397.
30 W.-W. Xu, Y. Chen, Y.-L. Lu, Y.-X. Qin, H. Zhang, X. Xu and Y. Liu, *Angew. Chem., Int. Ed.*, 2022, **61**, e202115265.
31 Y. Luo, W. Zhang, Q. Ren, Z. Tao and X. Xiao, *ACS Appl. Mater. Interfaces*, 2022, **14**, 29806–29812.
32 X. M. Chen, K. W. Cao, H. K. Bisoyi, S. Zhang, N. Qian, L. Guo, D. S. Guo, H. Yang and Q. Li, *Small*, 2022, **18**, e2204360.
33 M. Huo, X.-Y. Dai and Y. Liu, *Angew. Chem., Int. Ed.*, 2021, **60**, 27171–27177.
34 L. Xu, Z. Wang, R. Wang, L. Wang, X. He, H. Jiang, H. Tang, D. Cao and B. Z. Tang, *Angew. Chem., Int. Ed.*, 2020, **59**, 9908–9913.
35 H.-J. Kim, D. R. Whang, J. Gierschner and S. Y. Park, *Angew. Chem., Int. Ed.*, 2016, **55**, 15915–15919.
36 Y. Sun, F. Guo, T. Zuo, J. Hua and G. Diao, *Nat. Commun.*, 2016, **7**, 12042.
37 Z. Xu, S. Peng, Y. Y. Wang, J. K. Zhang, A. I. Lazar and D. S. Guo, *Adv. Mater.*, 2016, **28**, 7666–7671.
38 S. Guo, Y. Song, Y. He, X. Y. Hu and L. Wang, *Angew. Chem., Int. Ed.*, 2018, **57**, 3163–3167.
39 X. H. Wang, N. Song, W. Hou, C. Y. Wang, Y. Wang, J. Tang and Y. W. Yang, *Adv. Mater.*, 2019, **31**, 1903962.
40 X.-M. Chen, Q. Cao, H. K. Bisoyi, M. Wang, H. Yang and Q. Li, *Angew. Chem., Int. Ed.*, 2020, **59**, 10493–10497.
41 S. Fu, X. Su, M. Li, S. Song, L. Wang, D. Wang and B. Z. Tang, *Adv. Sci.*, 2020, **7**, 2001909.
42 M. Hao, G. Sun, M. Zuo, Z. Xu, Y. Chen, X.-Y. Hu and L. Wang, *Angew. Chem., Int. Ed.*, 2020, **59**, 10095–10100.
43 Y. Li, Y. Dong, L. Cheng, C. Qin, H. Nian, H. Zhang, Y. Yu and L. Cao, *J. Am. Chem. Soc.*, 2019, **141**, 8412–8415.
44 R.-Z. Zhang, Y.-S. Bi, K.-K. Niu, S. Yu, H. Liu and L.-B. Xing, *Adv. Opt. Mater.*, 2025, **13**, 2402112.
45 Y. Wang, N. Han, X. L. Li, R. Z. Wang and L. B. Xing, *ACS Appl. Mater. Interfaces*, 2022, **14**, 45734–45741.
46 Y. Wang, C.-Q. Ma, X.-L. Li, R.-Z. Dong, H. Liu, R.-Z. Wang, S. Yu and L.-B. Xing, *J. Mater. Chem. A*, 2023, **11**, 2627–2633.
47 X.-Z. Yang, Z.-G. Zhang, C.-L. Xin, H. Liu, S. Yu and L.-B. Xing, *J. Colloid Interface Sci.*, 2025, **680**, 587–595.
48 X. Li, S. Yu, Z. Shen, R. Wang, W. Zhang, A. Núñez-Delgado, N. Han and L.-B. Xing, *J. Colloid Interface Sci.*, 2022, **617**, 118–128.
49 H.-Q. Peng, Y.-Z. Chen, Y. Zhao, Q.-Z. Yang, L.-Z. Wu, C.-H. Tung, L.-P. Zhang and Q.-X. Tong, *Angew. Chem., Int. Ed.*, 2012, **51**, 2088–2092.
50 G. Chadha, Q.-Z. Yang and Y. Zhao, *Chem. Commun.*, 2015, **51**, 12939–12942.
51 J. Huang, Y. Yu, L. Wang, X. Wang, Z. Gu and S. Zhang, *ACS Appl. Mater. Interfaces*, 2017, **9**, 29030–29037.
52 J. Lou, X. Tang, H. Zhang, W. Guan and C. Lu, *Angew. Chem., Int. Ed.*, 2021, **60**, 13029–13034.
53 Y. Liu, J. Jin, H. Deng, K. Li, Y. Zheng, C. Yu and Y. Zhou, *Angew. Chem., Int. Ed.*, 2016, **55**, 7952–7957.
54 X. Li, Y. Wang, A. Song, M. Zhang, M. Chen, M. Jiang, S. Yu, R. Wang and L. Xing, *Chin. J. Chem.*, 2021, **39**, 2725–2730.
55 T. Sahin, M. A. Harris, P. Vairaprakash, D. M. Niedzwiedzki, V. Subramanian, A. P. Shreve, D. F. Bocian, D. Holten and J. S. Lindsey, *J. Phys. Chem. B*, 2015, **119**, 10231–10243.
56 H. Li, Y. Liu, T. Huang, M. Qi, Y. Ni, J. Wang, Y. Zheng, Y. Zhou and D. Yan, *Macromol. Rapid Commun.*, 2017, **38**, 1600818.
57 C. D. Bosch, J. Jevric, N. Burki, M. Probst, S. M. Langenegger and R. Haner, *Bioconjugate Chem.*, 2018, **29**, 1505–1509.
58 C. Vijayakumar, K. Sugiyasu and M. Takeuchi, *Chem. Sci.*, 2011, **2**, 291–294.
59 Q. Song, S. Goia, J. Yang, S. C. L. Hall, M. Staniforth, V. G. Stavros and S. Perrier, *J. Am. Chem. Soc.*, 2020, **143**, 382–389.
60 L. Ji, Y. Sang, G. Ouyang, D. Yang, P. Duan, Y. Jiang and M. Liu, *Angew. Chem., Int. Ed.*, 2019, **58**, 844–848.
61 Q. Zhang, X. Dang, F. Cui and T. Xiao, *Chem. Commun.*, 2024, **60**, 10064–10079.
62 Z. Wu, H. Qian, X. Li, T. Xiao and L. Wang, *Chin. Chem. Lett.*, 2023, **35**, 108829.
63 K. Wang, Y. Shen, P. Jeyakkumar, Y. Zhang, L. Chu, R. Zhang and X.-Y. Hu, *Curr. Opin. Green Sustainable Chem.*, 2023, **41**, 100823.
64 X.-M. Chen, X. Chen, X.-F. Hou, S. Zhang, D. Chen and Q. Li, *Nanoscale Adv.*, 2023, **5**, 1830–1852.
65 K. Wang, K. Velmurugan, B. Li and X.-Y. Hu, *Chem. Commun.*, 2021, **57**, 13641–13654.
66 Y. X. Hu, W. J. Li, P. P. Jia, X. Q. Wang, L. Xu and H. B. Yang, *Adv. Opt. Mater.*, 2020, **8**, 2000265.

